

Spatiotemporal variations of albedo in managed agricultural landscapes: Inferences to global warming impacts (GWI)

Pietro Sciusco^{1,2*}, Jiquan Chen^{1,2}, Michael Abraha^{2,3,4}, Cheyenne Lei^{1,2}, G. Philip Robertson^{3,4}, Raffaele Lafortezza^{5,6,2}, Gabriela Shirkey^{1,2}, Zutao Ouyang⁷, Rong Zhang^{8,9}, Ranjeet John¹⁰

¹ Department of Geography, Environment & Spatial Sciences, Michigan State University, East Lansing, MI, 48823, USA

²Center for Global Change and Earth Observations, Michigan State University, East Lansing, MI, 48823, USA

12 ³ Great Lakes Bioenergy Research Center, Michigan State University, East Lansing, MI, 48824, USA

13 ⁴ W.K. Kellogg Biological Station, Michigan State University, Hickory Corners, MI, 49060, USA

14 ⁵Department of Agricultural and Environmental Sciences, University of Bari “A. Moro”, Bari, 70126,
15 Italy

16 ⁶Department of Geography, The University of Hong Kong, Centennial Campus, Pokfulam Road, Hong
17 Kong

18 ⁷ Department of Earth System Science, Stanford University, Stanford, CA, 94305, USA

⁸ Zhejiang Tiantong Forest Ecosystem National Observation and Research Station, School of Ecological and Environmental Sciences, East China Normal University, Shanghai, 200241, China

⁹ Center for Global Change and Ecological Forecasting, East China Normal University, Shanghai, 200062, China

23 ¹⁰Department of Biology, University of South Dakota, Vermillion, SD, 57069, USA

24

25 * Corresponding author: Pietro Sciusco; Email: sciuscop@msu.edu; Phone: 517-505-1074

26 Date of manuscript revision: 02/19/2020

27 **Abstract**

28 **Context**

29 Albedo can be used to quantify ecosystem and landscape contributions to local and global climate.
30 Such contributions are conventionally expressed as radiative forcing (RF) and global warming impact
31 (GWI). We contextualize our results within landscape carbon production and storage to highlight the
32 importance of changes in albedo for landscape GWI from multiple causes, including net ecosystem
33 production (NEP) and greenhouse gas (GHG) emissions.

34 **Objective**

35 To examine the spatiotemporal changes in albedo ($\Delta\alpha$) in contrasting managed landscapes through
36 calculations of albedo-induced RF ($RF_{\Delta\alpha}$) and GWI ($GWI_{\Delta\alpha}$) under different climatic conditions.

37 **Methods**

38 We selected five contrasting landscapes within the Kalamazoo River watershed in southern Michigan
39 USA as proof of concept. The daily MCD43A3 MODIS (V006) product was used to analyze the inter-
40 and intra-annual variations of growing season albedo. In addition, the variations of $RF_{\Delta\alpha}$ and $GWI_{\Delta\alpha}$ were
41 computed based on landscape composition and climate.

42 **Results**

43 The $RF_{\Delta\alpha}$ (-5.6 W m^{-2}) and $GWI_{\Delta\alpha}$ ($-1.3 \text{ CO}_{2\text{eq}} \text{ ha}^{-1} \text{ yr}^{-1}$) were high in forest-dominated landscapes,
44 indicating cooling effects and $\text{CO}_{2\text{eq}}$ mitigation impacts similar to crops. The $\text{CO}_{2\text{eq}}$ mitigation of
45 cropland-dominated landscapes was on average 52% stronger than forest-dominated landscapes. In the
46 landscape with the highest proportion of forest, under dry and wet conditions $\text{CO}_{2\text{eq}}$ mitigation was
47 reduced by up to 24% and ~30%, respectively; in one cropland-dominated landscape wet conditions
48 reduced $\text{CO}_{2\text{eq}}$ mitigation by 23%.

49 **Conclusions**

50 Findings demonstrate that quantifying spatiotemporal changes in albedo in managed landscapes and
51 under different climatic conditions is essential to understand how landscape modification affects $RF_{\Delta\alpha}$ and
52 $GWI_{\Delta\alpha}$ and thereby contributes to ecosystem-level GWI.

53 **Keywords:** *Albedo, Land mosaics, Radiative forcing, Global warming impact, Cropland, Forest*

54 **1. Introduction**

55 Decoupling the causes and consequences of ecosystem functions and services at multiple spatial
56 scales represents an important scientific frontier in landscape ecology (Raudsepp-Hearne et al. 2010;
57 Antón et al. 2011; Chen et al. 2013; Yuan and Chen 2015; Seidl et al. 2016). Land use and land cover
58 change (LULCC) caused by human activities (e.g., land use), natural disturbances (e.g., wildfires) and
59 global warming directly affects regional and global climate through the exchange of energy, carbon,
60 water, and greenhouse gases (GHGs) between the land surface and the atmosphere (Bright et al. 2015;
61 Bonan 2016). Management activities and disturbances such as cultivation, burning, and grazing not only
62 influence GHG emissions but also alter the surface radiation balance (Pielke et al. 2011; Shao et al. 2014).
63 Unfortunately, little effort has been directed towards investigating resulting changes in surface radiation
64 balance (e.g., changes in albedo) at landscape scales (Euskirchen et al. 2002; Chen et al. 2004).

65 Albedo — the ratio of solar radiation reflected by a surface to the total incoming solar radiation (e.g.,
66 surface radiation balance) — is a measurable physical variable that can be used to quantify ecosystem and
67 landscape contributions to local and global climate (Dickinson 1983; Picard et al. 2012; Brovkin et al.
68 2013; Li et al. 2016; Storelvmo et al. 2016). Changing albedo has been proposed as one of several
69 geoengineering options for climate change mitigation (Lenton and Vaughan 2009; Goosse 2015) and
70 albedo is also important for understanding exchanges of energy and mass between terrestrial surfaces and
71 the atmosphere (Merlin 2013). Albedo is in its early stages of incorporation into climate models, but it is
72 useful for deriving different mechanisms to lower climate warming by potentially increasing the
73 reflectance of energy back into the atmosphere (Lenton and Vaughn 2009). Although LULCC (e.g.,
74 conversions from forest to biofuel, grassland, and cropland) can significantly alter albedo (Bala et al.
75 2007; Cai et al. 2016), the magnitude of changes depends on vegetation type and canopy structure (see
76 also Bennett et al. 2006; Tian et al. 2018).

77 Albedo is also highly correlated with leaf wetness, soil moisture, and soil water content (Henderson-
78 Sellers & Wilson 1983; Wang et al. 2004) — which are strongly related to precipitation and its temporal
79 distribution — and as well with plant phenology and vegetation structure (Luyssaert et al. 2014), plant or

80 tree height (Betts, 2001), and agricultural practices (Houspanossian et al. 2017) — this last scarcely
81 considered (Zhang et al. 2013, Jeong et al. 2014). For example, Culf et al. (1995) reported decreased
82 albedo in forests as a function of darker leaves and darker soils under wet conditions. Berbet and Costa
83 (2003) found that ranchlands were characterized by variable albedo throughout the entire year depending
84 on climatic conditions (e.g., dry vs wet periods), whereas forests were characterized by higher and lower
85 albedo in both dry and wet periods, respectively.

86 Changes in atmospheric conditions and land mosaics due to LULCC can affect the Earth's radiation
87 balance (Gray 2007). Radiative forcing (RF) has been widely used to describe this imbalance as changes
88 in the fraction of solar energy reflected by the Earth's surface (Mira et al. 2015), whether anthropogenic
89 or natural (Lenton and Vaughan 2009). RF can thus be used to compare modifications in radiation
90 balance due to atmospheric/surface albedo changes or due to GHG emissions. Previous studies (Betts
91 2000; Akbari et al. 2009) have developed methodologies to relate RF to $\text{CO}_{2\text{eq}}$, used to calculate
92 ecosystem-scale contributions to global warming impacts (GWIs) — a common measure for quantifying
93 RFs of different GHGs and other agents (Fuglestvedt et al. 2003; Forster et al. 2007; Peters et al. 2011).
94 GWI allows us to directly relate anthropogenic activities to GHG emissions (Haines 2003; Davin et al.
95 2007; Cherubini et al. 2012; Robertson et al. 2017) and to understand and quantify the impact of an
96 ecosystem on climate.

97 Despite escalating efforts to examine the magnitude and dynamics of albedo change due to LULCC,
98 previous studies have focused on albedo, RF, and GWI differences among the cover types within
99 landscapes or regions (Haas et al. 2001; Román et al. 2009; Carrer et al. 2018; Chen et al. 2019). For
100 example, previous studies have shown that deforestation and expanding agricultural lands have played an
101 important role in surface cooling of the northern hemisphere due to increased surface albedo and
102 regeneration of forests after harvesting (Betts 2001; Govindasamy et al. 2001; Lee et al. 2011). Georgescu
103 et al. (2011) simulated strong cooling effects — equivalent to a reduction in carbon emission of 78 t C ha^{-1}
104 ¹ — by increasing the surface albedo of agricultural lands across the central United States. Loarie et al.
105 (2011) demonstrated that introducing sugar cane production into cropland/pasture landscapes of Brazil

106 increased albedo and evapotranspiration, which in turn appeared to cool the local climate. Importantly, to
107 quantify the contribution of LULCC to global warming/cooling, GWI should be computed with reference
108 to albedo due to pre-existing conditions (i.e., $\Delta\alpha$).

109 Here we examine the spatiotemporal changes of albedo in contrasting managed landscapes as
110 compared to pre-existing forests through calculations of albedo-induced RF ($\Delta RF_{\Delta\alpha}$) and GWI ($\Delta GWI_{\Delta\alpha}$)
111 under different precipitation regimes (i.e., climatic conditions). We express the relationship between
112 landscape albedo and $\Delta GWI_{\Delta\alpha}$ (Figure 1) as:

$$113 [\Delta\alpha_i \times \Delta area_l \times \Delta climate_l] \rightarrow \Delta RF_{\Delta\alpha} \rightarrow \Delta GWI_{\Delta\alpha} \quad (1)$$

114 where $\Delta GWI_{\Delta\alpha}$ is net landscape albedo-induced GWI, $\Delta\alpha_i$ is the difference between mean albedo at a
115 cover type i and mean forest albedo (i.e., the reference), $\Delta area_l$ is variation of cover-type proportion for
116 landscape l , and $\Delta climate_l$ is the variation of climatic conditions for landscape l . More specifically, we
117 aim to estimate the magnitude and seasonal changes in albedo so that $\Delta GWI_{\Delta\alpha}$ can be assessed at
118 ecosystem, landscape, and watershed scales, and included in ecosystem GWI assessments (e.g., Gelfand
119 and Robertson 2015). We further contextualize our results within landscape carbon production and
120 storage to highlight the importance of changes in landscape $\Delta GWI_{\Delta\alpha}$ from multiple causes, including net
121 ecosystem production (NEP) and GHG emissions. The framework developed in this study (Equation 1,
122 Figure 1) can be applied to any landscape to for compute landscape $\Delta GWI_{\Delta\alpha}$. To this end, we selected five
123 contrasting landscapes in the Kalamazoo River watershed of southwestern Michigan U.S.A. as a proof of
124 concept to investigate inter- and intra-annual variations of albedo under three different climatic
125 conditions.

126 **2. Materials and Methods**

127 *2.1 Study area*

128 We chose five contrasting landscapes (Figure 2) in the Kalamazoo River watershed, located in
129 southwest Michigan, USA, for proof of concept. Within the 526,100 ha watershed, the long-term mean
130 annual temperature is 9.9 °C and the average annual precipitation is 900 mm that is evenly distributed

131 throughout the year (Michigan State Climatologist's Office 2013). The watershed includes portions of 10
132 counties: Allegan, Ottawa, Van Buren, Kent, Barry, Kalamazoo, Calhoun, Eaton, Jackson, and Hillsdale.
133 Prior to European settlement, the watershed was dominated by forests (Brown et al. 2000) with
134 interspersed tallgrass prairies, savannas, lakes, wetlands, and oak openings (Chapman and Brewer 2008).
135 The watershed however has undergone significant LULCC since then. Present-day forest areas are
136 secondary successional forests that followed their complete harvest by European settlers in the late 1800s
137 (Brown et al. 2000). Today, the watershed consists of cultivated crops, deciduous forest stands, pasture-
138 hay grasslands, inland lakes, wooded wetlands, and urban areas. Dominant soils of the watershed are
139 Alfisols of medium to coarse texture that allows a continuous recharge of groundwater (Schaetzl et al.
140 2009).

141 We randomly selected five 10,000 ha landscapes (Figure 2) (Burton et al. 1998) that represent the
142 main ecoregions of the watershed, i.e., areas characterized by similar vegetation, with the same type,
143 quality and quantity of environmental resources (Omernik and Griffith 2014). The Kalamazoo River
144 watershed includes three U.S. EPA ecoregions: Eastern Temperate Forest (Level I), Mixed Wood Plain
145 (Level II), and Southern Michigan/Northern Indiana Drift Plain (Level III). At a finer scale, five Level IV
146 ecoregions (Table S1) exist in the watershed: Battle Creek Outwash Plain (56b), Michigan Lake Plain
147 (56d), Lake Michigan Moraines (56f), Lansing Loamy Plain (56g), and Interlobate Dead Ice Moraines
148 (56h). (<https://www.epa.gov/eco-research/ecoregion-download-files-state-region-5#pane-20>). We used
149 the five landscapes to represent the five Level IV ecoregions so that each landscape fell within an
150 individual Level IV ecoregion.

151 Each landscape has different proportions of urban, cropland, barren, forest, water, wetland, and
152 grassland cover types (Table 1). Two of the five landscapes have a higher proportion of forest (FOR_1
153 highest proportion of forest, and FOR_2 second highest proportion); while the remaining three landscapes
154 are dominated by cropland ($CROP_1$, $CROP_2$, and $CROP_3$, from high to low proportion of cropland,
155 respectively) (Table 1). Given that forest was the dominant land cover type prior to European settlement
156 within each landscape (Brown et al. 2000), we considered the average albedo of all forest portions within

157 each of the five landscapes during the growing season at 10:30 a.m. local time (UTC) as the reference
158 albedo (e.g., MODIS Terra morning overpass time). Thereafter, in each landscape, changes in albedo ($\Delta\alpha$)
159 were obtained by calculating the difference between mean cropland and mean forest albedos, and then
160 used to calculate $RF_{\Delta\alpha}$ and $GWI_{\Delta\alpha}$.

161 *2.2 Landscape structure*

162 The landscape structure of the watershed was quantified from a classified land cover map for 2011
163 (Figure 2) at 30×30 m spatial resolution, which was produced using the Landsat archives from the USGS
164 Earth Explorer/GLOVIS portals (<https://earthexplorer.usgs.gov/>). The land cover map was obtained
165 following the Anderson level I classification scheme and included seven land cover types: 1) urban, 2)
166 cropland, 3) barren, 4) forest, 5) water, 6) wetland, and 7) grassland. The details of the accuracy
167 assessment (i.e., producer and user's accuracy for each class type and the overall accuracy in an error
168 matrix) of the classification were provided in Chen et al. (2019).

169 *2.3 MODIS Albedo*

170 Albedo datasets were obtained from the most recent collection (V006) of the MCD43A3 MODIS
171 Bidirectional Reflectance Distribution Function (BRDF) product
172 (<https://doi.org/10.5067/MODIS/MCD43A3.006>). MCD43A3 is a daily product at 500×500 m spatial
173 resolution obtained by inversion of a Bidirectional Reflectance Distribution Function (the BRDF) model
174 against a 16-day moving window of MODIS observations. The BRDF model was then used to derive the
175 black-sky (associated to direct solar radiation) and white-sky (associated to diffuse radiation) albedos
176 (Wang et al. 2018). We only considered snow-free, white-sky albedo at a shortwave length of 0.3-5.0 μm
177 (hereafter, α_{SHO} and expressed in percentage). For each image, the “Albedo_WSA_shortwave” (white-sky
178 albedo) band was selected and rescaled to 0-1. Only high-quality data were selected within the “full
179 BRDF inversion” quality band (QA = 0). The “Snow_BRDF_Albedo” band in the MCD43A2 product
180 was used to filter and exclude pixels with snow albedo retrievals (Chrysoulakis et al. 2018).

181 2.4 MODIS NDVI

182 Previous studies (e.g., Campbell and Norman 1998; Bonan 2008; Iqbal 2012; Liang et al. 2013; Zhao
183 and Jackson 2014; Bright et al. 2015; Kaye and Quemada 2017; Sun et al. 2017) have thoroughly
184 addressed the importance of snow cover on variability/uncertainty of albedo. Here, we focused on albedo
185 change, $RF_{\Delta a}$ and $GWI_{\Delta a}$ only during the growing season when maximum variability of watershed crop
186 phenology can be related with changes in climatic conditions and human disturbances at the landscape
187 level. Therefore, for each year, we identified the “growing season” during March-October by detecting
188 the greenness onset/offset for the entire Kalamazoo River watershed. To do so, for each year, we used a
189 16-day composite time series of the normalized difference vegetation index (NDVI) to detect the
190 inflection points (i.e., dates) when the maximum and minimum change rate of NDVI occurred (Jeong et
191 al. 2011). We obtained NDVI at a 250×250 m spatial resolution from the most recent collection (V006) of
192 the MYD13Q1 MODIS product (<https://doi.org/10.5067/MODIS/MYD13Q1.006>). Finally, we divided
193 each growing season (March-October) into three periods (hereafter, seasons) — spring, summer, and fall
194 using astronomical season (e.g., spring equinox, summer solstice, and fall equinox).

195 2.5 Precipitation data

196 Daily precipitation data at a 4×4 km spatial resolution were obtained from the Parameter-elevation
197 Regressions on Independent Slopes Model group (PRISM) AN81d product
198 (<http://www.prism.oregonstate.edu/>) over the 2012-2017 time period. We also calculated the cumulative
199 precipitation of the five landscapes during the growing season from March through October. For the time
200 period considered (e.g., 2012-2017), we then identified three years as dry, normal and wet years: 2012,
201 2017 and 2016, respectively. The Midwest of U.S.A. experienced 6 weeks of summer drought during
202 June-July in 2012 (Mallya et al. 2013), resulting in a growing season precipitation of <490 mm. In 2017,
203 the watershed received over 750 mm, while this was ~700 mm (i.e., near average) for 2016. All analysis
204 and processing of albedo, NDVI, and precipitation data were performed on the Google Earth Engine

205 (GEE) platform (Gorelick et al. 2017), where the MODIS products were uploaded, filtered to the date of
206 interest, and clipped to the shape file for each of the five landscapes.

207 *2.6 Statistical analysis*

208 We performed analysis of variance (ANOVA) to examine the change in albedo with land cover type
209 and landscape structure within the three-year study period and across three seasons. The following linear
210 model was applied:

211
$$\alpha_{SHO} = \text{landscape} \times \text{cover type} \times \text{year} \times \text{seasons} \quad (2)$$

212 where α_{SHO} is the snow-free white-sky albedo at the shortwave length at a daily step acquired from
213 MODIS at 10:30 a.m. local time (UTC); landscape, cover type, year, and season are the five landscapes
214 ($FOR_1, FOR_2, CROP_1, CROP_2, CROP_3$), the seven cover types (Table 1) at each landscape, the three
215 years (dry, wet, and normal), and the three astronomical seasons (spring, summer, and fall), respectively.

216 We also considered the interaction terms among the independent variables in our ANOVA.

217 To test the normality of our data we checked the distribution of the residuals. We then carried out
218 ANOVA and Tukey tests for multiple comparisons using the R-package ‘lsmeans’ (R Core Team 2017).

219 *2.7 Radiative forcing (RF) and global warming impact (GWI)*

220 To quantify the potential of RF caused by changes in albedo, we referred to the direct albedo-induced
221 RF at the top-of-atmosphere ($RF_{\Delta\alpha}$), where $\Delta\alpha$ is the change of α_{SHO} (i.e., the absolute difference between
222 mean cropland and mean forest albedos in each of the five landscapes). We calculated $RF_{\Delta\alpha}$ (W m^{-2})
223 following the algorithms of Carrer et al. (2018):

224
$$RF_{\Delta\alpha}(t) = -\frac{1}{N} \sum_{d=1}^N SW_{in} T_a \Delta\alpha \quad (3)$$

225 where $RF_{\Delta\alpha}$ is the mean albedo-induced radiative forcing at the top-of-atmosphere over the growing
226 season (t), N is the number of days in the growing season, SW_{in} is the incoming solar radiation at the
227 surface, T_a is the upward atmospheric transmittance and $\Delta\alpha$ is the albedo difference (i.e., between mean
228 cropland and mean forest albedos). By multiplying both SW_{in} and $\Delta\alpha$ by T_a , we calculated the

229 instantaneous amount of radiation that leaves the atmosphere at 10:30 a.m. UTC. It is worth reiterating
230 that all the variables (i.e., SW_{in} , $\Delta\alpha$, and T_a) refer to the specific time of 10:30 a.m. UTC (e.g., MODIS
231 Terra morning overpass time) and were considered to represent daily means. Negative values of $RF_{\Delta\alpha}$
232 indicate a cooling effect due to the differences between mean cropland and mean forest albedos.

233 While previous studies (e.g., Lenton and Vaughan 2009; Cherubini et al. 2012) used a global annual
234 average value of 0.854 for T_a , we calculated T_a as the ratio of incoming solar radiation at the top of the
235 atmosphere (SW_{TOA}) to that at the surface (SW_{in}) at 10:30 a.m. UTC. By assuming a same value of upward
236 and downward atmospheric transmittances (Carrer et al. 2018), SW_{in} (W m^{-2}) was obtained from a local
237 eddy covariance (EC) tower located at the Kellogg Biological Station Long-term Ecological Research site
238 (42°24'N, 85°24'W) (Abraha et al. 2015), while SW_{TOA} (W m^{-2}) was calculated as:

239
$$SW_{TOA} = S_{po} \cos(\theta) d \quad (4)$$

240 where S_{po} is the solar constant ($1,360 \text{ W m}^{-2}$), $\cos(\theta)$ is the cosine of the solar zenith angle, obtained from
241 the MCD43A2 (V006) MODIS BRDF Albedo Quality product
242 (<https://doi.org/10.5067/MODIS/MCD43A2.006>), applying the “BRDF_Albedo_LocalSolarNoon” band,
243 and d is the mean Earth-Sun distance. We then converted RF into the CO₂ equivalent (CO_{2eq}) by using the
244 GWI algorithms of Bird et al. (2008) and Carrer et al. (2018):

245
$$GWI_{\Delta\alpha}(t) = \frac{S RF_{\Delta\alpha}(t)}{AF rf_{CO_2}} \frac{1}{TH} \quad (5)$$

246 where $GWI_{\Delta\alpha}$ is the CO_{2eq} ($\text{kg CO}_{2eq} \text{ m}^{-2} \text{ yr}^{-1}$) GWI due to $\Delta\alpha$, represented by MODIS α_{SHO} acquisitions at
247 10:30 a.m. UTC, i.e., assuming that the values represent the mean CO_{2eq} mitigation impact of each
248 landscape during the growing season March-October (t), $RF_{\Delta\alpha}$ is the mean RF due to $\Delta\alpha$ over the growing
249 season March-October (t) (Equation 3), S is cropland area (ha) for which we hypothesized the change of
250 albedo occurred, AF is the CO₂ airborne fraction (0.48, Muñoz et al. 2010) obtained from the exponential
251 CO₂ decay function (see Bird et al. 2008 for more details), and TH is the time horizon of potential global
252 warming fixed at 100 years (Kaye and Quemada 2017). Lastly, the parameter rf_{CO_2} — the marginal RF of

253 CO₂ emissions at the current atmospheric concentration — is kept as a constant (Muñoz et al. 2010;
254 Bright et al. 2015; Carrer et al. 2018) at 0.908 W kg CO₂⁻¹.

255 Negative values of $GWI_{\Delta\alpha}$ indicate CO_{2eq} mitigation. We calculated the annual $GWI_{\Delta\alpha}$ as 1/100 of the
256 total CO_{2eq} to normalize to the 100 year time horizon used in the Kyoto Protocol (Boucher et al. 2009).

257 Notably, here we assumed that the same land mosaic in each landscape will be maintained for the
258 duration of 100 years. Previous studies (Betts 2000; Akbari et al. 2009) have also used a constant AF as
259 opposed to the exponential CO₂ decay function; however, the computed GWIs are similar (Bright 2015).

260 **3. Results**

261 Two of the five landscapes (FOR₁ and FOR₂) were dominated by forests (Table 1), with a forest
262 coverage of 57.5% in FOR₁ and 38.4% in FOR₂. Wetlands and croplands accounted for 16.9% and 10.5%
263 of landscape, respectively, in FOR₁ (Table 1), but only 10.1% and 26% in FOR₂ where urban land was
264 also the highest (13.3%). Croplands were dominant in CROP₁, CROP₂, and CROP₃ (Table 1), with
265 68.1%, 64.5%, and 57.2% of area coverage, respectively. Forest cover ranked the second highest in these
266 landscapes (14.2%, 16.7%, and 14.8%, respectively). Bare soils, grasslands, and water accounted for
267 small portions of all five landscapes.

268 The entire watershed had an α_{SHO} of 15.9% during the dry (2012) and wet (2016) years and of 15.6%
269 during the normal (2017) year (Table S2), yielding an overall average of 15.8% with a low inter-annual
270 variation. Each cover type contributed differently to α_{SHO} at the watershed level. In particular, croplands
271 and water bodies showed the highest (16.6%) and lowest (12.1%) α_{SHO} , respectively, with the highest
272 values occurring in both 2012 (16.6%±1.0) and 2016 (16.6%±1.1) for croplands, and the lowest in 2017
273 (11.9%±3.4) for water. The other cover types showed similar α_{SHO} values, ranging 15.1-15.6% for barren
274 and grassland, 15.2% for urban and forests and 15.4% for wetlands. At the landscape level, α_{SHO} of forest,
275 which was considered as reference, was generally lower than that of croplands. In particular, FOR₁ and
276 FOR₂ averaged a low α_{SHO} of 14.6% and 13.9%, respectively, whereas CROP₁, CROP₂, and CROP₃
277 recorded higher values of 16.7%, 16.4%, and 16.2%, respectively. However, FOR₁ and FOR₂

278 demonstrated the highest α_{SHO} in 2012 (14.7% \pm 0.8 and 14.1% \pm 2.3, respectively), while CROP₁, CROP₂,
279 and CROP₃ demonstrated the highest α_{SHO} in different years, such as 2016 for CROP₁ (17.0% \pm 0.8), 2012
280 and 2016 for CROP₂ (16.5% \pm 0.6), and 2017 for CROP₃ (16.3% \pm 1.7). In the forest-dominated landscapes,
281 all cover types showed higher α_{SHO} during the dry year (2012). However, for FOR₂, α_{SHO} values of
282 cropland and barren were high in the wet year (2016). In the cropland-dominated landscapes, the highest
283 α_{SHO} value (17.1%) was observed in CROP₃ (\pm 1.1) for croplands in 2017, and in CROP₁ for both urban
284 (\pm 0.6) and croplands (\pm 0.8) in 2016.

285 Our ANOVA model ($R^2=0.64$) (Table 2) indicated that the variation of α_{SHO} was significant (p-value
286 <0.001) among the five landscapes (i.e., ecoregions) ($\omega^2=26.6\%$) by cover type (i.e., landscape mosaics)
287 ($\omega^2=11.1\%$) and their interactions ($\omega^2=5.2\%$), with year and its interactions explaining $<1\%$ of the
288 variation. However, the variation from season (i.e., seasonality) ($\omega^2=15.9\%$) explained more than cover
289 type.

290 Forest-dominated landscapes (FOR₁ and FOR₂) showed lower least square means (LSM) of α_{SHO}
291 (LSM α_{SHO}) than cropland-dominated landscapes (CROP₁, CROP₂ and CROP₃) (Figure 3a) over the three
292 years. A decreasing inter-annual trend (between 2012, 2016, and 2017 growing seasons) characterized
293 FOR₁, FOR₂, and CROP₂, with FOR₁ showing statistically higher LSM α_{SHO} in the dry (2012) year;
294 whereas CROP₂ showed statistically lower LSM α_{SHO} in the normal (2017) year. In addition, differences in
295 LSM between cropland and forest albedos (LSM $_{\Delta\alpha}$) appeared to be higher in FOR₁, FOR₂, and CROP₃
296 (Figure 3b), but with increasing inter-annual trends, than in CROP₁ and CROP₂. However, only FOR₂
297 showed statistically lower LSM $_{\Delta\alpha}$ in the dry year (2012) (Figure 3b).

298 Clear seasonal patterns existed in α_{SHO} and were generally lower in spring and autumn than in the
299 summer (Figure 4). However, in CROP₂, the α_{SHO} of the major cover types (i.e., cropland, forest, urban,
300 and wetland) was the highest in the spring of the dry year. The α_{SHO} of cropland and urban areas in 2017
301 (a normal year) was also relatively higher in both spring and summer (Figures 4c₁–c₃). The inter-annual
302 variability between the wet and normal years (Figures 4b₁–b₄ and 4c₁–c₄, respectively) appeared similar,

303 with small differences between FOR_1 and FOR_2 (e.g., the lowest α_{SHO} occurring in spring in FOR_1 and in
304 autumn in FOR_2).

305 The mean $\Delta\alpha$ ranged between 0.4% and 2% (i.e., $\sim 1.2\%$ mean difference between mean cropland and
306 mean forest albedos) (Figure 4 Δ a– Δ c); however, the intra-annual variability of $\Delta\alpha$ differed by landscape
307 and year. We found that forest-dominated landscapes (FOR_1 and FOR_2) had higher $\Delta\alpha$ in spring each
308 year, with the minimum in autumn (FOR_1) and summer (FOR_2) of every year. Cropland-dominated
309 landscapes ($CROP_1$, $CROP_2$ and $CROP_3$, $CROP_3$) showed higher $\Delta\alpha$ in spring that was more pronounced
310 in 2016 for $CROP_1$ (Figure 4 Δ b), in 2016 and 2017 for $CROP_2$ (Figure 4 Δ b– Δ c), and in 2012 for $CROP_3$
311 (Figure 4 Δ a). However, $CROP_2$ in 2012 was characterized by a different $\Delta\alpha$ trend — lower in spring and
312 higher in autumn (Figure 4 Δ a). The summer $\Delta\alpha$ variability among the five landscapes was lower in the
313 dry year (Figure 4 Δ a) and higher in the normal year (Figure 4 Δ c). Two distinct clusters characterized the
314 summer of the wet year (Figure 4 Δ b), with FOR_1 , FOR_2 and $CROP_3$ having an $\Delta\alpha$ of $\geq 1\%$ and $CROP_1$
315 and $CROP_2$ of $\leq 0.5\%$.

316 All five landscapes had negative $RF_{\Delta\alpha}$ (Table 3; Figure 5a). Among the cropland-dominated
317 landscapes, $CROP_1$ and $CROP_2$ had similar lower magnitude $RF_{\Delta\alpha}$ values, with minimum and maximum
318 values in the wet (2016) and normal (2017) years, respectively. In particular, $CROP_2$ had $RF_{\Delta\alpha}$ ($W\ m^{-2}$) of
319 -1.2 in 2016 and -1.9 in 2017, followed by $CROP_1$ (-1.3 and -2.0) and $CROP_3$ (-2.9 and -3.7). Among the
320 forest-dominated landscapes, FOR_1 showed a similar trend, with minimum and maximum magnitude
321 $RF_{\Delta\alpha}$ in 2016 and 2017 (-3.9 and -5.6, respectively), while FOR_2 had the minimum and maximum
322 magnitude $RF_{\Delta\alpha}$ in the dry (2012) and normal (2017) years (-2.7 and -2.9, respectively).

323 As for $RF_{\Delta\alpha}$, all five landscapes showed negative values of $GWI_{\Delta\alpha}$ (Table 3; Figure 5b), which had
324 inter- and intra-annual trends similar to $RF_{\Delta\alpha}$ (Figure 5b). In particular, $CROP_1$ and $CROP_2$ had similar
325 lower magnitude $GWI_{\Delta\alpha}$ ($Mg\ CO_{2eq}\ ha^{-1}\ yr^{-1}$) values, with minimum ($CROP_1$ and $CROP_2$: -0.3) and
326 maximum ($CROP_1$: -0.5 and $CROP_2$: -0.4) values in the wet (2016) and normal (2017) years, respectively,
327 followed by $CROP_3$ (-0.7 and -0.9, respectively). FOR_1 showed a similar trend, with minimum and
328 maximum magnitude $GWI_{\Delta\alpha}$ in 2016 and 2017 (-0.9 and -1.3, respectively), with statistically higher

329 GWI_{Δα} in 2017, while FOR₂ had the minimum and maximum magnitude GWI_{Δα} in the dry (2012) and
330 both wet and normal (2016 and 2017) years (-0.6 and -0.7, respectively) (Table 3; Figure 5b).

331 Taking the normal year (2017) as our baseline, the percentage changes between the normal and dry
332 years (e.g., diff₂₀₁₇₋₂₀₁₂), and the normal and wet years (e.g., diff₂₀₁₇₋₂₀₁₆) showed reduced Δα, RF_{Δα}, and
333 GWI_{Δα} values (Table 3). In particular, the decrease in Δα was higher in FOR₂, CROP₁ CROP₂ (28.5%,
334 9.2%, and 19.4%, respectively) for diff₂₀₁₇₋₂₀₁₂ and in CROP₁ and CROP₂ (12.6% and 34.3%, respectively)
335 for diff₂₀₁₇₋₂₀₁₆. FOR₂ decreased the least from baseline in both RF_{Δα} and GWI_{Δα} compared to all other
336 landscapes, which had the highest decrease in diff₂₀₁₇₋₂₀₁₆ — FOR₁ (29.9%), CROP₁ (32.1%), CROP₂
337 (33.4%), and CROP₃ (23.3%). Statistically, reductions in Δα, RF_{Δα}, and GWI_{Δα} values were all significant
338 in FOR₁ (for both diff₂₀₁₇₋₂₀₁₂ and diff₂₀₁₇₋₂₀₁₆) and in CROP₂ (for diff₂₀₁₇₋₂₀₁₆).

339 **4. Discussion**

340 The main finding of our study is that RF_{Δα} and GWI_{Δα} play an important role in climate change
341 impact due to landscape mosaics. In particular, we found that forests have lower albedo than croplands,
342 which is in consistent with previous studies. In all five landscapes LULCC from forest to cropland
343 showed a cooling effect with negative RF_{Δα} and GWI_{Δα} values. The results also show that the difference
344 between mean cropland and mean forest albedos during the three years produces on average ~64%, 65%,
345 and 28% stronger CO_{2eq} mitigation impacts in the landscape with the highest proportion of forest (FOR₁)
346 than in cropland-dominated landscapes (CROP₁, CROP₂, and CROP₃, respectively), presumably due to
347 the lower proportion in cropland (e.g., 10.5% of cropland area) in FOR₁. Additionally, dry climatic
348 conditions in 2012 result in the highest albedo in almost all landscapes, although only significantly higher
349 in one of the forest-dominated (FOR₁) landscapes, supporting a consensus that dry surfaces reflect more
350 than wet surfaces. Over the growing season, albedo peaks in summer in all cover types, with lower albedo
351 in spring and autumn due to changes in plant phenology.

352 *4.1 Inter- and intra-annual changes in albedo*

353 We compared α_{SHO} values among major cover types (i.e., urban, cropland, forest, and wetland),
354 disregarding those with lower proportions (i.e., grassland, water, and barren) due to their negligible
355 contributions to the total landscape α_{SHO} . We observed that croplands and forests had on average 7.8%
356 higher and 0.7% lower albedo than other land covers, respectively. This is in line with previous studies
357 that examined snow-free albedo variations among ecosystems (Jiao et al. 2017, Chen et al. 2019) and
358 across the conterminous United States (Barnes and Roy 2010). Bonan (2008) showed that forests have
359 lower surface albedo than other cover types, contributing to climate warming. Our study indicated that in
360 forest-dominated landscapes (FOR₁ and FOR₂) the average of inter-annual variation of α_{SHO} was ~2.8%
361 lower than that in cropland-dominated landscapes (Table S2; Figure 3a). Analysis of variance also
362 revealed that the five landscapes (i.e., ecoregions), cover types (i.e., landscape mosaics), and seasons (i.e.,
363 seasonality) contributed significantly to the overall variation of α_{SHO} . Specifically, we found that besides
364 the five landscapes, seasons (~16%) contributed by 5% more than cover type (11%) towards variation of
365 α_{SHO} (Table 2).

366 Changes in α_{SHO} due to LULCC have been widely studied (Chrysoulakis et al. 2018); however, its
367 dynamics at ecosystem-to-landscape scales remain unexplored. For example, Zheng et al. (2019)
368 investigated how vegetation changes affect albedo trends without considering the integrated effect of both
369 cover type and seasonality, while Matthews et al. (2003) investigated the cooling/warming effects of
370 albedo change resulting from deforestation, but failed to consider realistic land cover change scenarios. A
371 number of agricultural management practices are known to mitigate climate change (summarized in
372 Smith et al. 2008 and Eagle et al. 2012), including GHG emission reductions and soil carbon storage, but
373 the potential contribution of albedo change as an ecosystem-scale mitigation factor has not been much
374 addressed. For example, tillage practices, harvest timing, residue management, and winter cover crops can
375 all affect surface reflectance in annual cropping systems (Bright et al. 2015; Poeplau and Don 2015; Kaye
376 and Quemada 2017; Robertson et al. 2017) and thus GWI.

377 To our knowledge, no effort has been made to understand albedo mitigation in terms of both RF and
378 GWI in the context of landscape mosaics characterized by diverse land use type and intensity. Using the
379 framework listed in Equation 1 and Figure 1, we were able to integrate spatial (e.g., five landscapes
380 within ecoregions) and temporal (e.g., inter- and intra-annual) changes as main drivers of α_{SHO} variations.
381 Regardless of land composition, cropland-dominated landscapes showed a higher intra-annual variability
382 of α_{SHO} than forests under dry, wet, and normal climatic conditions (Figure 4 a–c), likely due to the higher
383 disturbances that croplands experience (i.e., fragmentation, land management, crop variety, and crop
384 seasonality). For example, α_{SHO} can be altered by the differences in leaf structure/properties (Miller et al.
385 2016) and leaf wetness (Luyssaert et al. 2014), by the difference in management of both perennial and
386 annual crops and by agricultural practices (Bright et al. 2015; Kaye and Quemada 2017; Robertson et al.
387 2017).

388 The LSM multi-comparison analysis showed that dry conditions led FOR_1 to yield statistically higher
389 α_{SHO} compared to wet and normal conditions. On the other hand, $CROP_2$ showed significantly lower α_{SHO}
390 under normal conditions than under dry and wet conditions (Figure 3a), indicating a different albedo
391 response of forest- and cropland-dominated landscapes to changes in climatic conditions. All other
392 landscapes showed higher α_{SHO} in the dry year (2012) than in the normal and wet years, although not
393 statistically different.

394 *4.2 Albedo-induced radiative forcing ($RF_{\Delta\alpha}$) and global warming impact ($GWI_{\Delta\alpha}$)*

395 We obtained $RF_{\Delta\alpha}$ ($W\ m^{-2}$) values that were more representative of the entire growing season through
396 the years 2012, 2016, and 2017. We found that the five landscapes had a negative $RF_{\Delta\alpha}$, indicating a
397 cooling effect. However, such effect was stronger in FOR_1 where it ranged between $-3.9\ W\ m^{-2}$ and $-5.6\ W\ m^{-2}$
398 (Table 3; Figure 5a), followed by $CROP_3$ ($-2.9\ W\ m^{-2}$ and $-3.7\ W\ m^{-2}$) and FOR_2 ($-2.7\ W\ m^{-2}$ and $-2.9\ W\ m^{-2}$), while $CROP_1$ and $CROP_2$ were almost similar (ranging between $-1.2\ W\ m^{-2}$ and $-1.9\ W\ m^{-2}$,
400 respectively). In other words, land mosaics in the landscape with the highest proportion of forest (e.g.,
401 FOR_1) leads to a maximum $RF_{\Delta\alpha}$ of $-5.6\ W\ m^{-2}$ (i.e., a cooling effect), which is similar to that

402 hypothesized by Jiao et al. (2017) under the simulated scenario of global deforestation of evergreen
403 broadleaf forests (local magnitude of RF_{TOA} at -5.6 W m^{-2}). Moreover, in this study we were able to
404 investigate $RF_{\Delta\alpha}$ dynamics across three contrasting precipitation regimes — dry (2012), wet (2016), and
405 normal (2017). The inter-annual analysis specifically showed that within each landscape, the cooling
406 effect was lower in 2016 and higher in 2017, with the exception of FOR_2 , which had a lower cooling
407 effect in 2012 and a higher one in 2017 (e.g., slightly higher than in 2016). In sum, accurate quantification
408 of landscape contribution to the global warming potentials needs input from both landscape composition
409 and climate that directly regulate ecosystem properties.

410 The $GWI_{\Delta\alpha}$ computations enabled us to estimate the CO_{2eq} mitigation caused by the differences
411 between mean cropland and mean forest albedos. Standardized to the same areas, the greatest contribution
412 of albedo change to GWI occurred in the FOR_1 ($GWI_{\Delta\alpha} = -1.3 \text{ Mg CO}_{2eq} \text{ ha}^{-1}$ in 2017; Table 3; Figure
413 5b), whereas the least contribution occurred in $CROP_2$ ($-0.3 \text{ Mg CO}_{2eq} \text{ ha}^{-1} \text{ yr}^{-1}$). These contributions to
414 GWI are of the same order of magnitude as many crop management components. For example, in this
415 same watershed a corn-soybean-wheat rotation managed with a legume cover crop had a net GWI of $0.4 -$
416 $0.6 \text{ Mg CO}_{2eq} \text{ ha}^{-1} \text{ yr}^{-1}$ (Robertson et al 2000), without considering albedo change due to historical
417 LULCC. Likewise, the net GWI of conventional and no-till cropping systems were similar in magnitude
418 without consideration of albedo; 0.3 to $0.9 \text{ Mg CO}_{2eq} \text{ ha}^{-1} \text{ yr}^{-1}$, respectively (Gelfand et al. 2013). In
419 several landscapes (FOR_1 , FOR_2 , and $CROP_3$), $GWI_{\Delta\alpha}$ was sufficient to offset the GWI costs of both N_2O
420 emissions ($0.4 \text{ Mg CO}_{2eq} \text{ ha}^{-1} \text{ yr}^{-1}$) and farming inputs for an alfalfa cropping system ($\sim 0.8 \text{ Mg CO}_{2eq} \text{ ha}^{-1}$
421 yr^{-1}) (Gelfand et al. 2013).

422 Surprisingly, the results of inter-annual variation among the three growing seasons showed that the
423 CO_{2eq} mitigation impact between forest- and cropland-dominated (FOR_1 , $CROP_3$) landscapes was
424 statistically different in 2012 and 2016 for FOR_1 (Table 3, Figure 5a) and in 2016 for $CROP_3$, suggesting
425 that changes in climate conditions, as seen in our study from dry to normal and from wet to normal, can
426 affect the CO_{2eq} mitigation impacts of landscapes. Overall, in one of the forest-dominated landscapes
427 (FOR_1) the percent decrease of CO_{2eq} mitigation due to dry and wet conditions was higher than that of the

428 cropland-dominated landscape CROP₃ under wet conditions (e.g., lower albedo). Specifically, we found
429 that both dry and wet conditions in FOR₁ could significantly reduce CO_{2eq} mitigation by up to 24% and
430 ~30% (i.e., percentage change), respectively; while the CO_{2eq} mitigation's decreasing in CROP₃ was
431 significant under wet conditions (e.g., 23.3%), which, in both cases, is still enough to offset 11% of the
432 total CO_{2eq} emissions of conventionally tilled corn systems in the same area and under the same climatic
433 conditions (i.e., 2012 and 2016) (Abraha et al. 2019). Surprisingly the high decrease in $\Delta\alpha$ (e.g., FOR₁:
434 9% vs 6.1% and CROP₃: 6% vs 1%) under wet conditions did not lead to a high decrease in CO_{2eq}
435 mitigation.

436 4.3 Assumptions, limitations and uncertainties

437 The methodology used in this study represents an analytical approach as a proof of concept of the
438 effects of landscape patches and climatic conditions on RF _{$\Delta\alpha$} and GWI _{$\Delta\alpha$} in the context of forest- and
439 cropland-dominant landscapes. However, certain assumptions can be made on the application of our
440 approach. The first is that RF _{$\Delta\alpha$} is related to land mosaics (e.g., patch composition) derived by land
441 transformation (Muñoz et al. 2010). In fact, the focus of the present study is to measure the changes in
442 RF _{$\Delta\alpha$} and GWI _{$\Delta\alpha$} due to conversion of forests to croplands, assuming the existing croplands were forests
443 in the past. We then considered $\Delta\alpha$ using the baseline (forest), which is treated as a reference cover type
444 of the five landscapes, since it was the dominant land cover type of the pre-European settlements (Brown
445 et al. 2000).

446 A second assumption is related to using *in-situ* incoming radiation (SW_{in}) for the calculation of
447 upward atmospheric transmittance (T_a). While the literature (Lenton and Vaughan 2009; Muñoz et al.
448 2010; Cherubini et al. 2012) refers to T_a as the annual global mean (T_a = 0.854) for a constant zenith
449 angle of 60°, here we calculated T_a for a given day as the ratio SW_{in}/SW_{TOA}, with SW_{in} obtained from *in-*
450 *situ* measurements within the study area (Abraha et al. 2015), specifically at the FOR₂ landscape. By
451 avoiding such a default value for T_a (e.g., 0.845), we reduced the error by ~30%. We then assumed that
452 SW_{in} would be the same at all five landscape locations. In fact, unlike previous studies, we calculated

453 RF_{Δα} and GWI_{Δα} on a relatively small area (i.e., not global/regional) for which the uncertainty error
454 carried by a constant T_a would not have been significant.

455 A third assumption is related to the time horizon (TH) fixed at 100 years, which is the same time
456 horizon used in the Kyoto Protocol (Boucher et al. 2009). By calculating the annual GWI_{Δα} as 1/100 of
457 the total CO_{2eq}, we assumed that, in each landscape, the same land mosaic will be maintained for the
458 duration of 100 years. This choice of TH is a limitation because short time horizons can overemphasize
459 the impacts of albedo, while long time horizons can de-emphasize the impacts (Anderson-Teixeira et al.
460 2012).

461 Another limitation of the study is the use of a growing season (March-October) time frame for RF_{Δα}
462 and GWI_{Δα} rather than an annual period. Previous studies (Campbell and Norman 1998; Bonan 2008;
463 Iqbal 2012; Liang et al. 2013; Zhao and Jackson 2014; Bright et al. 2015; Kaye and Quemada 2017; Sun
464 et al. 2017) have addressed the importance of snow cover to variability/uncertainty of albedo between
465 forest and cropland because of the capability of forest stands of masking the snow (e.g., lowing the
466 albedo). Nevertheless, our use of growing season values allowed to better isolate the human disturbance
467 on the landscape through agricultural activities by focusing on the crop phenology and its relation with
468 climatic conditions. Had we included wintertime albedo, our forest-cropland differences would have been
469 even greater, however, since deciduous forest stands have higher wintertime albedo than cropland due to
470 the presence of bare branches (Bonan 2008; Anderson et al. 2011) during winter. On the other hand, from
471 the remote sensing perspective, MODIS snow-albedo retrievals have been demonstrated to be less
472 accurate than acquisitions during the growing season (Wang et al., 2014).

473 There are also uncertainties associated with user-defined data (Muñoz et al. 2010), such as
474 considering Δα as the difference between croplands and forest albedos. AF (i.e., CO₂ airborne fraction)
475 and rf_{CO₂} (the marginal RF of CO₂ emissions at the current atmospheric concentration) are estimated to
476 embed errors of ±15% and ±10%, respectively, in the GWI estimation (Forster et al. 2007; Akbari et al.
477 2009). It is also worth mentioning the uncertainties related to the scale-dependency. In fact, there is a
478 mismatch between the spatial representativeness of MODIS acquisition pixels (e.g., 500×500 m) and that

479 of Landsat (30×30 m), which leads to intrinsic variability of the measurements (Chrysoulakis et al. 2018;
480 Chen et al. 2019). However, as already emphasized in previous studies (Mira et al. 2015; Moustafa et al.
481 2017), validation techniques provide a reasonable estimate of albedo from MODIS products across
482 homogeneous landscapes (e.g., the two forest- and the three cropland-dominated landscapes).

483 Lastly, we did not consider the effect of spatial autocorrelation that may affect the significance of the
484 statistic test (Fletcher and Fortin 2018). Nevertheless, the aim of this study is not to attempt spatial
485 predictions (Feilhauer et al. 2012) of $RF_{\Delta\alpha}$ and $GWI_{\Delta\alpha}$.

486 **5. Conclusions**

487 1. There are significant contributions ($R^2=0.64$) to the overall variation in albedo due to landscapes
488 (i.e., ecoregions), cover types (i.e., landscape mosaics), and seasons (i.e., seasonality). Variation in
489 seasons contributes more than landscape composition (~16% and 11%, respectively) in variations of
490 albedo.

491 2. By integrating spatial (e.g., five landscapes within ecoregions) and temporal (e.g., inter- and intra-
492 annual) patterns as main drivers of albedo variation, we found that cropland-dominated landscapes
493 produce a higher intra-annual variability of albedo under dry, wet, and normal climatic conditions, likely
494 due to more frequent disturbances (i.e., management activities). Forest-dominated landscapes have higher
495 albedo in dry and wet years than that in normal years, whereas only one crop-dominated landscape shows
496 statistically lower albedo under normal conditions than that under dry and wet ones. This indicates a
497 different response to changes in climatic conditions from forest- and cropland-dominated landscapes.

498 3. The cooling effect of $RF_{\Delta\alpha}$ occurs in all landscapes but is higher in the landscape with the highest
499 proportion of forests (FOR_1) (e.g., higher differences between mean cropland and mean forest albedos).
500 The pattern of $GWI_{\Delta\alpha}$ across the five landscapes is similar to that of $RF_{\Delta\alpha}$, with CO_{2eq} mitigation relative
501 to pre-existing forest vegetation higher in FOR_1 and lower in $CROP_1$ and $CROP_2$.

502 4. We found that in the landscape with the highest proportion of forest (FOR_1) both dry and wet
503 conditions can significantly reduce CO_{2eq} mitigation by up to 24% and ~30%, respectively; while the

504 reduction of CO_{2eq} mitigation is significant only in one of the cropland-dominated landscapes (CROP₃)
505 under wet conditions (e.g., 23.3% decrease).

506 **Acknowledgements:** This study was supported, in part, by the NASA Carbon Cycle & Ecosystems
507 program (NNX17AE16G), the Great Lakes Bioenergy Research Center funded by the U.S. Department of
508 Energy, Office of Science, Office of Biological and Environmental Research under Award Numbers DE-
509 SC0018409 and DE-FC02-07ER64494 and the Natural Science Foundation Long-term Ecological
510 Research Program (DEB 1637653) at the Kellogg Biological Station, the NASA Science of Terra and
511 Aqua program (NNX14AJ32G). We wish to thank Dr. Geoffrey Henebry for helpful suggestions and
512 comments during the post-review process. We also thank the two anonymous reviewers who helped
513 improving the quality of our manuscript.

514 **References**

515 Abraha M, Chen J, Chu H, et al (2015) Evapotranspiration of annual and perennial biofuel crops in a
516 variable climate. *Glob Change Bio Bioenergy* 7:1344–1356. <https://doi.org/10.1111/gcbb.12239>

517 Abraha M, Gelfand I, Hamilton SK, et al (2016) Ecosystem water-use efficiency of annual corn and
518 perennial grasslands: contributions from land-use history and species composition. *Ecosystems*
519 19:1001–1012. <https://doi.org/10.1007/s10021-016-9981-2>

520 Abraha M, Gelfand I, Hamilton SK, et al (2019) Carbon debt of field-scale conservation reserve program
521 grasslands converted to annual and perennial bioenergy crops. *Environ Res Lett* 14:024019.
522 <https://doi.org/10.1088/1748-9326/aafc10>

523 Akbari H, Menon S, Rosenfeld A (2009) Global cooling: increasing world-wide urban albedos to offset
524 CO₂. *Clim Change* 94:275–286. <https://doi.org/10.1007/s10584-008-9515-9>

525 Anderson RG, Canadell JG, Randerson JT, et al (2011) Biophysical considerations in forestry for climate
526 protection. *Front Ecol Environ* 9:174–182. <https://doi.org/10.1890/090179>

527 Anderson-Teixeira KJ, Snyder PK, Twine TE, et al (2012) Climate-regulation services of natural and
528 agricultural ecoregions of the Americas. *Nat Clim Change* 2:177–181.
529 <https://doi.org/10.1038/nclimate1346>

530 Antón A, Cebrian J, Heck KL, et al (2011) Decoupled effects (positive to negative) of nutrient enrichment
531 on ecosystem services. *Ecol Appl* 21:991–1009. <https://doi.org/10.1890/09-0841.1>

532 Bala G, Caldeira K, Wickett M, et al (2007) Combined climate and carbon-cycle effects of large-scale
533 deforestation. *Proc Natl Acad Sci* 104:6550–6555. <https://doi.org/10.1073/pnas.0608998104>

534 Barnes CA, Roy DP (2010) Radiative forcing over the conterminous United States due to contemporary
535 land cover land use change and sensitivity to snow and interannual albedo variability. *J Geophys Res
536 Biogeosciences* 115:G04033. <https://doi.org/10.1029/2010JG001428>

537 Bennett AF, Radford JQ, Haslem A (2006) Properties of land mosaics: implications for nature
538 conservation in agricultural environments. *Biol Conserv* 133:250–264.
539 <https://doi.org/10.1016/j.biocon.2006.06.008>

540 Berbet MLC, Costa MH (2003) Climate change after tropical deforestation: seasonal variability of surface
541 albedo and its effects on precipitation change. *J Clim* 16:2099–2104. [https://doi.org/10.1175/1520-0442\(2003\)016<2099:CCATDS>2.0.CO;2](https://doi.org/10.1175/1520-0442(2003)016<2099:CCATDS>2.0.CO;2)

543 Betts RA (2000) Offset of the potential carbon sink from boreal forestation by decreases in surface
544 albedo. *Nature* 408:187–190. <https://doi.org/10.1038/35041545>

545 Betts RA (2001) Biogeophysical impacts of land use on present-day climate: near-surface temperature
546 change and radiative forcing. *Atmospheric Sci Lett* 2:39–51. <https://doi.org/10.1006/asle.2001.0037>

547 Bird DN, Kunda M, Mayer A, et al (2008) Incorporating changes in albedo in estimating the climate
548 mitigation benefits of land use change projects. *Biogeosciences Discuss* 5:1511–1543.
549 <https://doi.org/10.5194/bgd-5-1511-2008>

550 Bonan GB (2008) Forests and climate change: forcings, feedbacks, and the climate benefits of forests.
551 *Science* 320:1444–1449. <https://doi.org/10.1126/science.1155121>

552 Bonan GB (2016) *Ecological Climatology: Concepts and Applications*. Cambridge University Press,
553 Cambridge 723p.

554 Boucher O, Friedlingstein P, Collins B, Shine KP (2009) The indirect global warming potential and
555 global temperature change potential due to methane oxidation. *Environ Res Lett* 4:044007.
556 <https://doi.org/10.1088/1748-9326/4/4/044007>

557 Bright RM (2015) Metrics for biogeophysical climate forcings from land use and land cover changes and
558 their inclusion in life cycle assessment: a critical review. *Environ Sci Technol* 49:3291–3303.
559 <https://doi.org/10.1021/es505465t>

560 Bright RM, Zhao K, Jackson RB, Cherubini F (2015) Quantifying surface albedo and other direct
561 biogeophysical climate forcings of forestry activities. *Glob Change Biol* 21:3246–3266.
562 <https://doi.org/10.1111/gcb.12951>

563 Brovkin V, Boysen L, Raddatz T, Gayler V, Loew A, Claussen M (2013) Evaluation of vegetation cover
564 and land-surface albedo in MPI-ESM CMIP5 simulations. *J Adv Model Earth SY* 5:48–57.
565 <https://doi.org/10.1029/2012MS000169>

566 Brown DG, Pijanowski BC, Duh JD (2000) Modeling the relationships between land use and land cover
567 on private lands in the Upper Midwest, USA. *J Environ Manage* 59:247–263.
568 <https://doi.org/10.1006/jema.2000.0369>

569 Cai H, Wang J, Feng Y, et al (2016) Consideration of land use change-induced surface albedo effects in
570 life-cycle analysis of biofuels. *Energy Environ Sci* 9:2855–2867.
571 <https://doi.org/10.1039/C6EE01728B>

572 Campbell GS, Norman JM (1998) *Introduction to Environmental Biophysics*, 2nd ed. Springer, New York
573 286p.

574 Carrer D, Pique G, Ferlicoq M, et al (2018) What is the potential of cropland albedo management in the
575 fight against global warming? A case study based on the use of cover crops. *Environ Res Lett*
576 13:044030. <https://doi.org/10.1088/17489326/aab650>

577 Chen J, Brosofske KD, Noormets A, et al (2004) A working framework for quantifying carbon
578 sequestration in disturbed land mosaics. *Environ Manage* 33:S210–S221.
579 <https://doi.org/10.1007/s00267-003-9131-4>

580 Chen J, Sciusco P, Ouyang Z, et al (2019) Linear downscaling from MODIS to Landsat: connecting
581 landscape composition with ecosystem functions. *Landscape Ecology* 34:2917–2934.
582 <https://doi.org/10.1007/s10980-019-00928-2>

583 Chen J, Wan S, Henebry G, et al (2013) *Dryland East Asia: Land Dynamics Amid Social and Climate*
584 *Change*. Walter de Gruyter, Berlin, Boston 470p.

585 Cherubini F, Bright RM, Strømman AH (2012) Site-specific global warming potentials of biogenic CO₂
586 for bioenergy: contributions from carbon fluxes and albedo dynamics. *Environ Res Lett* 7:045902.
587 <https://doi.org/10.1088/1748-9326/7/4/045902>

588 Chrysoulakis N, Mitraka Z, Gorelick N (2018) Exploiting satellite observations for global surface albedo
589 trends monitoring. *Theor Appl Climatol* 137:1171–1179. <https://doi.org/10.1007/s00704-018-2663-6>

590 Culf AD, Fisch G, Hodnett MG (1995) The albedo of Amazonian forest and ranch land. *J Clim* 8:1544–
591 1554. [https://doi.org/10.1175/1520-0442\(1995\)008<1544:TAOAFA>2.0.CO;2](https://doi.org/10.1175/1520-0442(1995)008<1544:TAOAFA>2.0.CO;2)

592 Davin EL, Noblet-Ducoudré N de, Friedlingstein P (2007) Impact of land cover change on surface
593 climate: relevance of the radiative forcing concept. *Geophys Res Lett* 34:L13702.
594 <https://doi.org/10.1029/2007GL029678>

595 Davin EL, Seneviratne SI, Ciais P, et al (2014) Preferential cooling of hot extremes from cropland albedo
596 management. *Proc Natl Acad Sci* 111:9757–9761. <https://doi.org/10.1073/pnas.1317323111>

597 Dickinson RE (1983) Land surface processes and climate—surface albedos and energy balance. In:
598 Saltzman B (ed) *Adv Geophys* 25:305–353. [https://doi.org/10.1016/S0065-2687\(08\)60176-4](https://doi.org/10.1016/S0065-2687(08)60176-4)

599 Eagle AJ, Henry LR, Olander LP, Haugen-Kozyra K, Millar N, Robertson GP (2010) *Greenhouse gas*
600 *mitigation potential of agricultural land management in the United States. A Synthesis of the*
601 *Literature*. Technical Working Group on Agricultural Greenhouse Gases (T-AGG) Report 68p.

602 Euskirchen ES, Chen J, Li H, et al (2002) Modeling landscape net ecosystem productivity (LandNEP)
603 under alternative management regimes. *Ecol Model* 154:75–91. [https://doi.org/10.1016/S0304-3800\(02\)00052-2](https://doi.org/10.1016/S0304-3800(02)00052-2)

604 Feilhauer H, He KS, Rocchini D (2012) Modeling species distribution using niche-based proxies derived
605 from composite bioclimatic variables and MODIS NDVI. *Remote Sens* 4:2057–2075.
606 <https://doi.org/10.3390/rs4072057>

607 Fletcher R, Fortin M-J (2018) *Spatial Dependence and Autocorrelation*. In: Fletcher R, Fortin M-J (eds)
608 *Spatial Ecology and Conservation Modeling: Applications with R*. Springer International Publishing,
609 Cham, pp 133–168

610 Forster P, Ramaswamy V, Artaxo P, et al (2007) Changes in atmospheric constituents and in radiative
611 forcing. In: *Climate Change 2007. The Physical Science Basis* 25:527–542.
612 <https://doi.org/10.1175/2011JCLI4183.1>

614 Fuglestvedt JS, Berntsen TK, Godal O, et al (2003) Metrics of climate change: assessing radiative forcing
615 and emission indices. *Clim Change* 58:267–331. <https://doi.org/10.1023/A:1023905326842>

616 Gelfand I, Sahajpal R, Zhang X, et al (2013) Sustainable bioenergy production from marginal lands in the
617 US Midwest. *Nature* 493:514–517. <https://doi.org/10.1038/nature11811>

618 Gelfand, I. and G. P. Robertson. 2015. Mitigation of greenhouse gas emissions in agricultural ecosystems.
619 Pages 310-339 in S. K. Hamilton, J. E. Doll, and G. P. Robertson, editors. *The Ecology of*
620 *Agricultural Landscapes: Long-Term Research on the Path to Sustainability*. Oxford University
621 Press, New York, New York, USA.

622 Georgescu M, Lobell DB, Field CB (2011) Direct climate effects of perennial bioenergy crops in the
623 United States. *Proc Natl Acad Sci* 108:4307–4312. <https://doi.org/10.1073/pnas.1008779108>

624 Goosse, H. (2015) *Climate System Dynamics and Modeling*. Cambridge University Press, Cambridge
625 357p

626 Gorelick N, Hancher M, Dixon M, et al (2017) Google Earth Engine: planetary-scale geospatial analysis
627 for everyone. *Remote Sens Environ* 202:18–27. <https://doi.org/10.1016/j.rse.2017.06.031>

628 Govindasamy B, Duffy PB, Caldeira K (2001) Land use changes and northern hemisphere cooling.
629 *Geophys Res Lett* 28:291–294. <https://doi.org/10.1029/2000GL006121>

630 Gray V (2007) Climate Change 2007: The physical science basis summary for policymakers. *Energy*
631 *Environ* 18:433–440. <https://doi.org/10.1260/095830507781076194>

632 Haas G, Wetterich F, Köpke U (2001) Comparing intensive, extensified and organic grassland farming in
633 southern Germany by process life cycle assessment. *Agric Ecosyst Environ* 83:43–53.
634 [https://doi.org/10.1016/S0167-8809\(00\)00160-2](https://doi.org/10.1016/S0167-8809(00)00160-2)

635 Haralick RM, Shanmugam K, Dinstein I (1973) Textural features for image classification. *IEEE Trans*
636 *Syst Man Cybern SMC* 3:610–621. <https://doi.org/10.1109/TSMC.1973.4309314>

637 Henderson-Sellers A, Wilson MF (1983) Surface albedo data for climatic modeling. *Rev Geophys*
638 21:1743–1778. <https://doi.org/10.1029/RG021i008p01743>

639 Houspanossian J, Giménez R, Jobbágy E, Noisetto M (2017) Surface albedo raise in the South American
640 Chaco: Combined effects of deforestation and agricultural changes. *Agric For Meteorol* 232:118–127.
641 <https://doi.org/10.1016/j.agrformet.2016.08.015>

642 Iqbal M (2012) *An Introduction to Solar Radiation*. Elsevier, 390p

643 Jeong SJ, Ho C-H, GIM HJ, Brown ME (2011) Phenology shifts at start vs. end of growing season in
644 temperate vegetation over the Northern Hemisphere for the period 1982–2008. *Glob Change Bio*
645 17:2385–2399. <https://doi.org/10.1111/j.1365-2486.2011.02397.x>

646 Jeong SJ, Ho C-H, Piao S, et al (2014) Effects of double cropping on summer climate of the North China
647 Plain and neighbouring regions. *Nat Clim Change* 4:615–619. <https://doi.org/10.1038/nclimate2266>

648 Jiao T, Williams CA, Ghimire B, et al (2017) Global climate forcing from albedo change caused by large-
649 scale deforestation and reforestation: quantification and attribution of geographic variation. *Clim
650 Change* 142:463–476. <https://doi.org/10.1007/s10584-017-1962-8>

651 Kaye JP, Quemada M (2017) Using cover crops to mitigate and adapt to climate change. A review. *Agron
652 Sustain Dev* 37:4. <https://doi.org/10.1007/s13593-016-0410-x>

653 Lee X, Goulden ML, Hollinger DY, et al (2011) Observed increase in local cooling effect of deforestation
654 at higher latitudes. *Nature* 479:384–387. <https://doi.org/10.1038/nature10588>

655 Lenton TM, Vaughan NE (2009) The radiative forcing potential of different climate geoengineering
656 options. *Atmos Chem Phys* 9:5539–5561. <https://doi.org/10.5194/acp-9-5539-2009>

657 Li J, Wang X, Wang X, et al (2009) Remote sensing evaluation of urban heat island and its spatial pattern
658 of the Shanghai metropolitan area, China. *Ecol Complex* 6:413–420.
659 <https://doi.org/10.1016/j.ecocom.2009.02.002>

660 Li B, Gasser T, Ciais P, et al (2016) The contribution of China's emissions to global climate forcing.
661 *Nature* 531(7594): 357. <https://doi.org/10.1038/nature17165>

662 Liang S, Zhao X, Liu S, et al (2013) A long-term Global LAnd Surface Satellite (GLASS) data-set for
663 environmental studies. *Int J Digit Earth* 6:5–33. <https://doi.org/10.1080/17538947.2013.805262>

664 Loarie SR, Lobell DB, Asner GP, et al (2011) Direct impacts on local climate of sugar-cane expansion in
665 Brazil. *Nat Clim Change* 1:105–109. <https://doi.org/10.1038/nclimate1067>

666 Luyssaert S, Jammet M, Stoy PC, et al (2014) Land management and land-cover change have impacts of
667 similar magnitude on surface temperature. *Nat Clim Change* 4:389–393.
668 <https://doi.org/10.1038/nclimate2196>

669 Mallya G, Zhao L, Song XC, et al (2013) 2012 Midwest drought in the United States. *J Hydrol Eng*
670 18:737–745. [https://doi.org/10.1061/\(ASCE\)HE.1943-5584.0000786](https://doi.org/10.1061/(ASCE)HE.1943-5584.0000786)

671 Matthews HD, Weaver AJ, Eby M, Meissner KJ (2003) Radiative forcing of climate by historical land
672 cover change. *Geophysical Res Lett* 30(2). <https://doi.org/10.1525/bio.2013.63.4.6>

673 Merlin O (2013) An original interpretation of the wet edge of the surface temperature-albedo space to
674 estimate crop evapotranspiration (SEB-1S), and its validation over an irrigated area in northwestern
675 Mexico. *Hydrol Earth Sys Sci* 17:3623–3637. <https://doi.org/10.5194/hess-17-3623-2013>

676 Michigan State Climatologist's Office (2013). *Gull Lake (3504)*. Michigan State University. Retrieved
677 from http://climate.geo.msu.edu/climate_mi/stations/3504/

678 Miller JN, VanLoocke A, Gomez-Casanovas N, Bernacchi CJ (2016) Candidate perennial bioenergy
679 grasses have a higher albedo than annual row crops. *Glob Change Biol Bioenergy* 8:818–825.
680 <https://doi.org/10.1111/gcbb.12291>

681 Mira M, Weiss M, Baret F, et al (2015) The MODIS (collection V006) BRDF/albedo product MCD43D:
682 Temporal course evaluated over agricultural landscape. *Remote Sens Environ* 170:216–228.
683 <https://doi.org/10.1016/j.rse.2015.09.021>

684 Moustafa SE, Rennermalm AK, Román MO, et al (2017) Evaluation of satellite remote sensing albedo
685 retrievals over the ablation area of the southwestern Greenland ice sheet. *Remote Sens Environ*
686 198:115–125. <https://doi.org/10.1016/j.rse.2017.05.030>

687 Muñoz I, Campra P, Fernández-Alba AR (2010) Including CO₂-emission equivalence of changes in land
688 surface albedo in life cycle assessment. Methodology and case study on greenhouse agriculture. *Int J*
689 *Life Cycle Assess* 15:672–681. <https://doi.org/10.1007/s11367-010-0202-5>

690 Omernik JM, Griffith GE (2014) Ecoregions of the conterminous United States: Evolution of a
691 hierarchical spatial framework. *Environ Manage* 54:1249–1266. <https://doi.org/10.1007/s00267-014-0364-1>

692

693 Peters GP, Aamaas B, T. Lund M, et al (2011) Alternative “global warming” metrics in life cycle
694 assessment: a case study with existing transportation data. *Environ Sci Technol* 45:8633–8641.
695 <https://doi.org/10.1021/es200627s>

696 Picard G, Domine F, Krinner G, et al (2012) Inhibition of the positive snow-albedo feedback by
697 precipitation in interior Antarctica. *Nat Clim Change* 2:795–798.
698 <https://doi.org/10.1038/nclimate1590>

699 Pielke RA, Pitman A, Niyogi D, et al (2011) Land use/land cover changes and climate: Modeling analysis
700 and observational evidence. *Wiley Interdiscip Rev Clim Change* 2:828–850.
701 <https://doi.org/10.1002/wcc.144>

702 Poeplau C, Don A (2015) Carbon sequestration in agricultural soils via cultivation of cover crops – a
703 meta-analysis. *Agric Ecosyst Environ* 200:33–41. <https://doi.org/10.1016/j.agee.2014.10.024>

704 Raudsepp-Hearne C, Peterson GD, Tengö M, et al (2010) Untangling the environmentalist’s paradox:
705 why is human well-being increasing as ecosystem services degrade? *BioScience* 60:576–589.
706 <https://doi.org/10.1525/bio.2010.60.8.4>

707 Robertson GP, Paul EA, Harwood RR (2000) Greenhouse gases in intensive agriculture: contributions of
708 individual gases to the radiative forcing of the atmosphere. *Science* 289:1922–1925.
709 <https://doi.org/10.1126/science.289.5486.1922>

710 Robertson GP, Hamilton SK, Barham BL, et al (2017) Cellulosic biofuel contributions to a sustainable
711 energy future: Choices and outcomes. *Science* 356:1349. <https://doi.org/10.1126/science.aal2324>

712 Román MO, Schaaf CB, Woodcock CE, et al (2009) The MODIS (collection V005) BRDF/albedo
713 product: assessment of spatial representativeness over forested landscapes. *Remote Sens Environ*
714 113:2476–2498. <https://doi.org/10.1016/j.rse.2009.07.009>

715 Seidl R, Spies TA, Peterson DL, et al (2016) Searching for resilience: Addressing the impacts of changing
716 disturbance regimes on forest ecosystem services. *J Appl Ecol* 53:120–129.
717 <https://doi.org/10.1111/1365-2664.12511>

718 Shao C, Li L, Dong G, Chen J (2014) Spatial variation of net radiation and its contribution to energy
719 balance closures in grassland ecosystems. *Ecol Process* 3:7. <https://doi.org/10.1186/2192-1709-3-7>

720 Smith P, Martino D, Cai Z, et al (2008) Greenhouse gas mitigation in agriculture. *Philosophical
721 Transactions of the Royal Society B: Biological Sciences* 363: 789–813. <https://doi.org/10.1098/rstb.2007.2184>

722 Storelvmo T, Leirvik T, Lohmann U, Phillips PC, Wild M (2016) Disentangling greenhouse warming and
723 aerosol cooling to reveal Earth's climate sensitivity. *Nature Geoscience* 9:286.
724 <https://doi.org/10.1038/NGEO2670>

725 Sun Q, Wang Z, Li Z, et al (2017) Evaluation of the global MODIS 30 arc-second spatially and
726 temporally complete snow-free land surface albedo and reflectance anisotropy dataset. *Int J Appl
727 Earth Obs Geoinformation* 58:36–49. <https://doi.org/10.1016/j.jag.2017.01.011>

728 Tian L, Chen J, Shao C (2018) Interdependent dynamics of LAI-albedo across the roofing landscapes:
729 Mongolian and Tibetan Plateaus. *Remote Sens* 10:1159. <https://doi.org/10.3390/rs10071159>

730 Wang D, Liang S, He T, et al (2015) Estimating daily mean land surface albedo from MODIS data. *J
731 Geophys Res Atmospheres* 120:4825–4841. <https://doi.org/10.1002/2015JD023178>

732 Wang K, Liu J, Zhou X, et al (2004) Validation of the MODIS global land surface albedo product using
733 ground measurements in a semidesert region on the Tibetan Plateau. *J Geophys Res Atmospheres*
734 109:D05107 <https://doi.org/10.1029/2003JD004229>

735 Wang Z, Schaaf CB, Strahler AH, et al (2014) Evaluation of MODIS albedo product (MCD43A) over
736 grassland, agriculture and forest surface types during dormant and snow-covered periods. *Remote
737 Sens Environ* 140:60–77. <https://doi.org/10.1016/j.rse.2013.08.025>

738 Yuan ZY, Chen HYH (2015) Decoupling of nitrogen and phosphorus in terrestrial plants associated with
739 global changes. *Nat Clim Change* 5:465–469. <https://doi.org/10.1038/nclimate2549>

740 Zhang Y, Wang X, Pan Y, Hu R (2013) Diurnal and seasonal variations of surface albedo in a spring
741 wheat field of arid lands of Northwestern China. *Int J Biometeorol* 57:67–73.
742 <https://doi.org/10.1007/s00484-012-0534-x>

743 Zhao K, Jackson RB (2014) Biophysical forcings of land-use changes from potential forestry activities in
744 North America. *Ecol Monogr* 84:329–353. <https://doi.org/10.1890/12-1705.1>

745 Zheng L, Zhao G, Dong J, et al (2019) Spatial, temporal, and spectral variations in albedo due to
746 vegetation changes in China's grasslands. *ISPRS J Photogramm Remote Sens* 152:1–12.
747 <https://doi.org/10.1016/j.isprsjprs.2019.03.020>

749 **Tables**750 **Table 1** Land cover composition of the five landscapes. Bold values indicate the cover type dominating
751 the landscape.

752

Cover type	Landscape				
	FOR ₁	FOR ₂	CROP ₁	CROP ₂	CROP ₃
	ha (%)				
Urban	513 (5.2)	1330 (13.3)	545 (5.5)	1047 (10.5)	1341 (13.4)
Cropland	1035 (10.5)	2597 (26.0)	6807 (68.1)	6442 (64.5)	5713 (57.2)
Barren	530 (5.4)	286 (2.9)	49 (0.5)	62 (0.6)	64 (0.6)
Forest	5672 (57.5)	3833 (38.4)	1415 (14.2)	1670 (16.7)	1477 (14.8)
Water	410 (4.2)	922 (9.2)	56 (0.6)	43 (0.4)	442 (4.4)
Wetland	1669 (16.9)	1012 (10.1)	1101 (11.0)	693 (6.9)	917 (9.2)
Grassland	30 (0.3)	12 (0.1)	21 (0.2)	35 (0.4)	38 (0.4)

753

Table 2 Statistical results of analysis of variance (ANOVA) based on the linear model in Equation 1 (dependent variable: α_{SHO}).

Variable	DF	SS	MS	F	p	ω^2	R ²
landscape	4	1.869	0.467	3689.660	***	0.266	
seasons	2	1.118	0.559	4414.651	***	0.159	
cover type	6	0.779	0.130	1024.423	***	0.111	
landscape × cover type	24	0.371	0.015	121.891	***	0.052	
landscape × seasons	8	0.142	0.018	140.167	***	0.020	
landscape × cover type × seasons	48	0.079	0.002	12.962	***	0.011	
year × seasons	4	0.048	0.012	94.672	***	0.007	
cover type × seasons	12	0.030	0.003	19.844	***	0.004	
landscape × year	8	0.022	0.003	21.210	***	0.003	
landscape × year × seasons	16	0.020	0.001	9.684	***	0.003	
year	2	0.013	0.007	51.367	***	0.002	
landscape × cover type × year	48	0.015	0	2.505	***	0.002	
cover type × year	12	0.002	0	1.278		0	
cover type × year × seasons	24	0.003	0	1.047		0	
landscape × cover type × year × seasons	96	0.011	0	0.887		0	0.64
Residuals	19779	2.505	0				

754
755

ω^2 indicates variance in the dependent variable α_{SHO} accounted for by the independent variables landscape, cover type, year, seasons, and their interactions. Significance codes: “***” p < 0.001, “**” p < 0.01, “*” p < 0.05, “.” p < 0.1, “ ” p > 0.1.

756 **Table 3** Mean change of $\Delta\alpha$ (%), $RF_{\Delta\alpha}$ ($W\ m^{-2}$), and $GWI_{\Delta\alpha}$ ($Mg\ CO_{2eq}\ ha^{-1}\ yr^{-1}$) for each landscape in 2012, 2016, and 2017 growing seasons.

757 Negative values for $RF_{\Delta\alpha}$ and $GWI_{\Delta\alpha}$ indicate cooling effects and CO_{2eq} mitigation impacts due to albedo change, respectively. Percentage changes
 758 (%) between 2017 (baseline) and the two extreme climatic years (i.e., $diff_{2017-2012}$ and $diff_{2017-2016}$, respectively) are also shown. Values with
 759 significant decrease (e.g., percent change) are highlighted in bold texts.

760

	2012			2016			2017			diff ₂₀₁₇₋₂₀₁₂		diff ₂₀₁₇₋₂₀₁₆	
	$\Delta\alpha$	$RF_{\Delta\alpha}$	$GWI_{\Delta\alpha}$	$\Delta\alpha$	$RF_{\Delta\alpha}$	$GWI_{\Delta\alpha}$	$\Delta\alpha$	$RF_{\Delta\alpha}$	$GWI_{\Delta\alpha}$	$\Delta\alpha$	$RF_{\Delta\alpha} / GWI_{\Delta\alpha}$	$\Delta\alpha$	$RF_{\Delta\alpha} / GWI_{\Delta\alpha}$
	FOR ₁	1.2 (± 0.8)	-4.2	-1.0	1.2 (± 0.8)	-3.9	-0.9	1.3 (± 0.6)	-5.6	-1.3	9.0	24.0	6.1
FOR ₂	0.8 (± 0.3)	-2.7	-0.6	1.0 (± 0.4)	-2.9	-0.7	1.1 (± 2.0)	-2.9	-0.7	28.5	9.0	7.8	1.4
CROP ₁	0.5 (± 0.2)	-1.7	-0.4	0.5 (± 0.3)	-1.3	-0.3	0.5 (± 0.3)	-2.0	-0.5	9.2	15.6	12.6	32.1
CROP ₂	0.5 (± 0.3)	-1.7	-0.4	0.4 (± 0.2)	-1.2	-0.3	0.6 (± 1.4)	-1.9	-0.4	19.4	9.9	34.3	33.4
CROP ₃	0.9 (± 0.3)	-3.2	-0.7	0.9 (± 0.6)	-2.9	-0.7	0.9 (± 0.5)	-3.7	-0.9	6.0	14.9	1.0	23.3

761 **Figure captions**

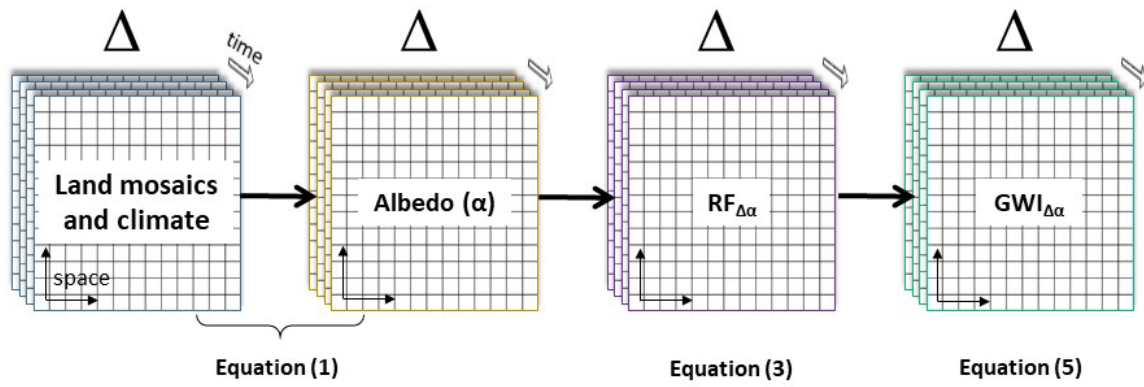
762 **Fig. 1** Schematic diagram showing the relationship between landscape albedo and $\text{GWI}_{\Delta\alpha}$.

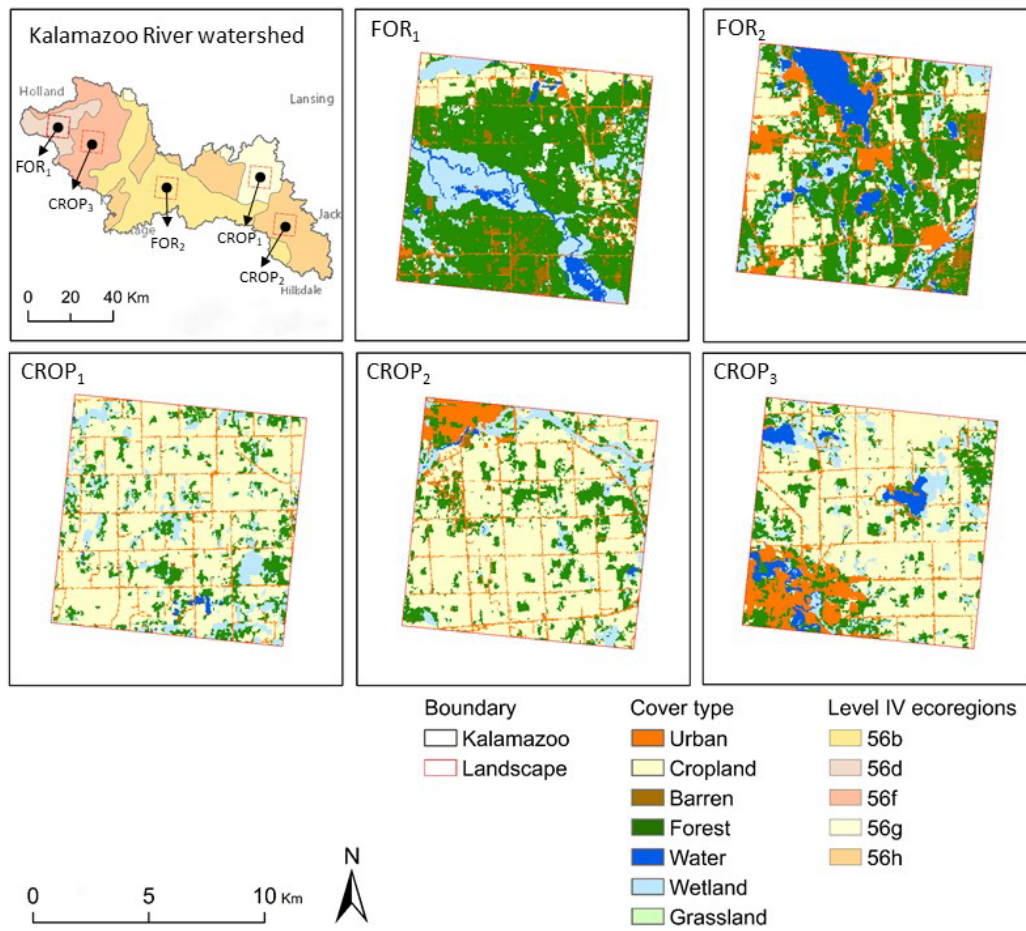
763 **Fig. 2** Locations of the five landscapes (FOR_1 , FOR_2 , CROP_1 , CROP_2 , CROP_3) within the Kalamazoo
764 River watershed in the southwest Michigan (USA). Each landscape falls within a unique Level IV
765 ecoregion defined by the United States Environmental Protection Agency (US EPA). Basemap sources:
766 *Esri, HERE, Garmin, USGS, Intermap, INCREMENT P, NRCAN, Esri Japan, METI, Esri China (Hong*
767 *Kong), NOSTRA, © OpenStreetMap contributors, and the GIS User Community.*

768 **Fig. 3** Least square means (LSM) multi-comparison analysis of α_{SHO} (a) and $\Delta\alpha_{\text{SHO}}$ (b) in 2012, 2016, and
769 2017 for each landscape. Boxes indicate the LSM; whiskers represent the lower and upper limits of the
770 95% family-wise confidence level of the LSM. Boxes sharing the same letters are not significantly
771 different (intra- and inter-annual, as well as within and among the five landscapes) according to the Tukey
772 HSD test.

773 **Fig. 4** Mean α_{SHO} (%) by cover type and season in 2012 (a₁–a₄), 2016 (b₁–b₄), and 2017 (c₁–c₄) for the
774 five landscapes. Mean of the difference between mean cropland and mean forest albedos ($\Delta\alpha_{\text{SHO}}$) for the
775 same years (Δa , Δb , and Δc , respectively) is also shown.

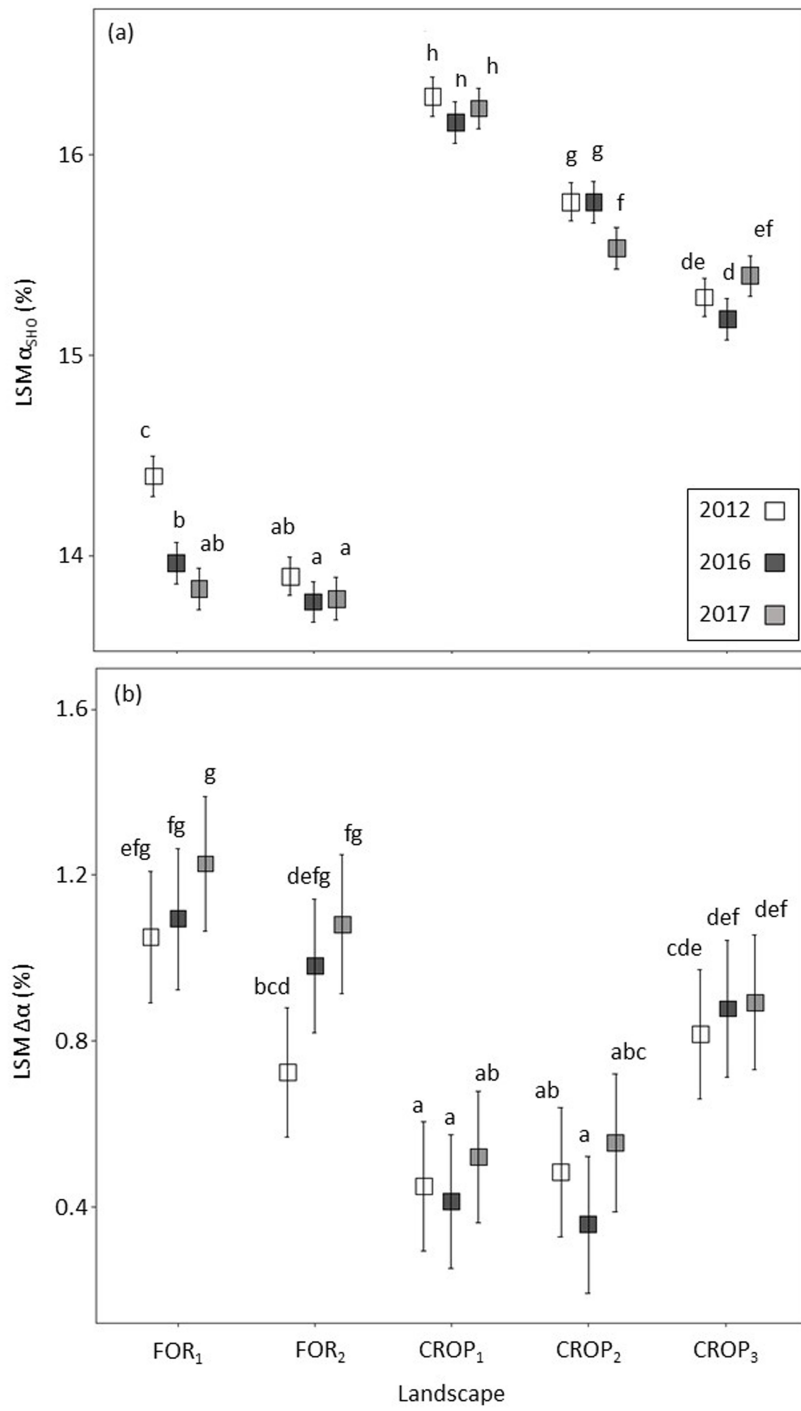
776 **Fig. 5** Bar chart of $\text{RF}_{\Delta\alpha}$ (W m^{-2}) due to the difference between mean cropland and mean forest albedos at
777 the top-of-atmosphere across five landscapes at 10:30 a.m. local time (UTC) during the 2012, 2016, and
778 2017 growing seasons (a). Panel (b) shows $\text{GWI}_{\Delta\alpha}$ ($\text{Mg CO}_{2\text{eq}} \text{ha}^{-1} \text{yr}^{-1}$) due to the difference between
779 mean cropland and mean forest albedos. Negative values for $\text{RF}_{\Delta\alpha}$ and $\text{GWI}_{\Delta\alpha}$ indicate cooling effects and
780 $\text{CO}_{2\text{eq}}$ mitigation impacts, respectively. Bars sharing the same letters are not significantly different (intra-
781 and inter-annual, as well as within and among the five landscapes) according to the Tukey HSD test.





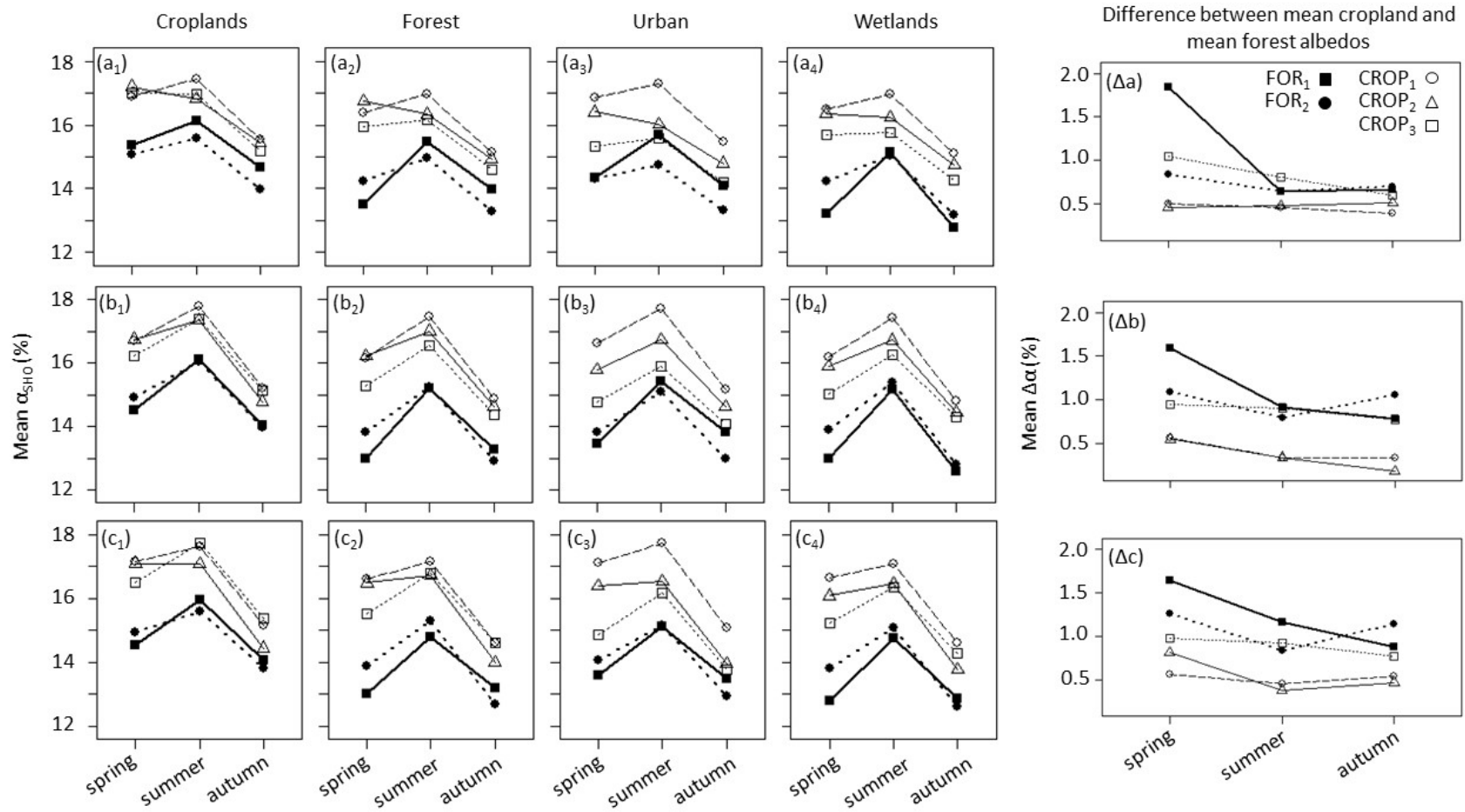
785

786 **Fig. 2**



787
788

Fig. 3



789

790 **Fig. 4**

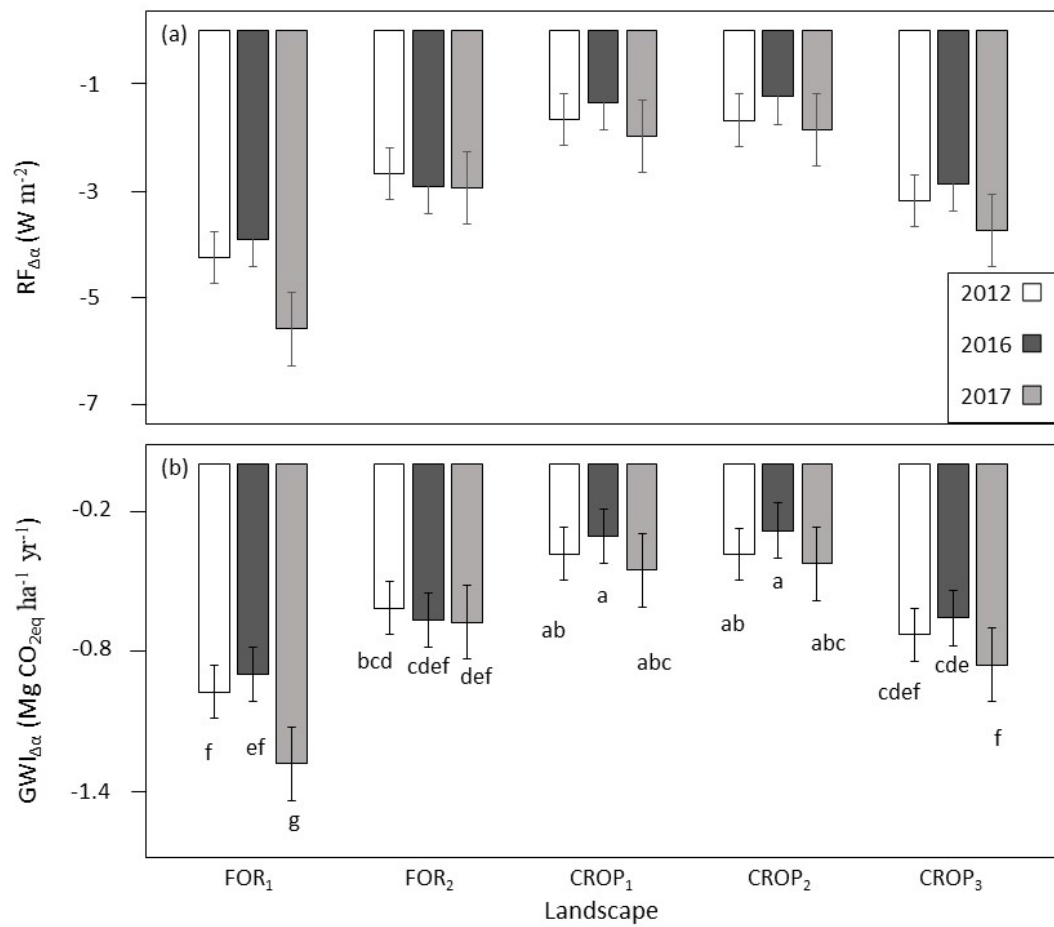


Fig. 5